Strojniški vestnik - Journal of Mechanical Engineering 61(2015)11, 741-750
DOI:10.5545/sv-jme.2015.2610
Original Scientific Paper
Received for review: 2015-04-16
Received revised form: 2015-07-17
Accepted for publication: 2015-09-02

Artificial Neural Networks to Estimate the Thermal Properties of an Experimental Micro-Alloyed Steel and Their Application to the Welding Thermal Analysis

Edgar López-Martínez[1,*] – Héctor Javier Vergara-Hernández[2] – Sergio Serna[3] – Bernardo Campillo[1,4]

[1] National Autonomous University of Mexico, Faculty of Chemistry, Mexico
[2] Morelia Institute of Technology, Metallurgy Science Postgraduate Programme, Mexico
[3] State Autonomous University of Morelos, Research Center in Engineering and Applied Sciences, Mexico
[4] National Autonomous University of Mexico, Institute of Physical Sciences, Mexico

The effect of welding thermal cycles on the microstructure and micro-hardness of the heat-affected zone (HAZ) of an experimental micro-alloyed steel was studied. Due to the experimental difficulties involved in acquiring the thermal cycles, these were determined by applying the solutions of Rosenthal's equations for thick and thin plates. However, to perform this thermal analysis, it requires knowledge of the thermal properties of the micro-alloyed steel; therefore, the implementation of two artificial neural networks (ANNs) was proposed as tool to estimate the thermal conductivity and the heat capacity as a function of the chemical composition and temperature. The ANNs were trained with information obtained from the literature review and then tested with steels that were not used for the training step, but with thermal properties known. A good approximation between the actual and the estimated properties was observed.

It was determined that the microstructural characteristics of the welding zone are a function of the thermal cycles, although there is no great difference in micro-hardness. Martensite was not observed in the welding zone; therefore, the welds of this steel, under these welding conditions, could not be susceptible to hydrogen induced cracking (HIC).

Keywords: heat capacity, thermal conductivity, micro-alloyed steel, heat-affected zone, artificial neural network

Highlights

- *The design of two artificial neural networks was proposed to determine the thermal properties as a function of the chemical composition and temperature of metallic materials.*
- *The thermal conductivity and heat capacity of metallic materials can be estimated as a function of temperature.*
- *The high temperatures reached in the coarse-grained heat-affected zone induced grain growth, which together with the high cooling rate (69 K/s), favoured the formation of bainite.*
- *There is no great difference in micro-hardness in the welding zone.*

0 INTRODUCTION

In manufacturing processes such as solidification, metal forming, welding and powder metallurgy, heat transfer phenomena are involved. For a suitable design and/or analysis of one of these processes, it is necessary to know the thermal properties of the materials. For example, in the heat treatment process designs, it is necessary to know the thermal conductivity and the heat capacity, since the thermal cycles that develop during the process will produce a microstructural change, which will affect the mechanical properties and mechanical behaviour.

Micro-alloyed steels or high-strength low-alloy steels are a special type of structural steels that obtain their outstanding final mechanical properties by thermomechanical treatments and accelerated cooling. However, to achieve a final shape or final component, such as in the field installation of pipelines, these steels are subjected to several welding thermal cycles, and then they can suffer several microstructural changes in the welding zone. Due to the experienced thermal cycles, the base material microstructure can be partially or completely modified to produce a fusion zone (FZ) or weld metal (WM), and a heat-affected zone (HAZ), which leads the welding zone to present different mechanical properties, toughness, and susceptibility to hydrogen-induced cracking (HIC) [1] to [3]. Moreover, mathematical modelling has become a powerful tool to analyse the effect of thermal cycles on the microstructure, mechanical properties, and mechanical behaviour of welded products [4], where it is necessary to know or estimate the thermal properties such as the thermal conductivity and the heat capacity. Usually, the thermal conductivity is determined at steady state by using the guarded-comparative-longitudinal heat-flow technique in heating and the heat capacity is determined at a high heating rate by using differential scanning calorimetry.

Artificial neural networks (ANNs) have been used to solve many problems, in the social and economic sciences as well as health sciences. In

*Corr. Author's Address: National Autonomous University of Mexico, Av. Universidad 3000, Mexico City 04510, Mexico, edgar0902@comunidad.unam.mx

metallurgy, ANNs have been used to model the transition temperature from ductile to brittle in steel [5]; the determination of static recrystallization of hot-deformed steels [6]; the determination of residual stress [7]; the correlation of processing parameters and properties [8]; the microstructural determinations [9]; predicting the behaviour of corrosion-fatigue [10]; modelling toughness of micro-alloyed steels [11]; predict migration energies of vacancies [12]; the prediction of the grain boundary energy [13], and the prediction of steel surface roughness [14]. In the welding process, ANNs have been used to predict the welding-induced angular distortion [15]; the occurrence in solidification cracking [16]; to calculate output parameters of friction-stir welding [17]; to predict the hardness of HAZ for in-service welded pipelines [18].

An ANN is a structure composed of nodes or neurons interconnected and arranged in layers to which weight factors are assigned . Each node in each layer is connected to other nodes in other layers by applying the sum of the weights in a transfer function. The basic architecture of an ANN is composed of three types of layers: input layer, hidden layer and output layer, although an ANN can have more than one hidden layer.

To build an ANN, a database is first required, which is divided into two parts: one for the training step and the other for the testing step. The training step consists of feeding the ANN with information from both the independent and dependent variables, i.e. the input neuron and output neuron signals. Each input is weighted and transformed by a transfer function. With the implementation of a learning rule, the weights of the input neurons are adjusted and the process is repeated until a minimum error is obtained between output neurons and the actual values, so it is said that the ANN has been trained. In the testing step, the ANN is fed with input neurons, but not with output neurons. If the results obtained with the ANN are similar to those actual values, it is said that the ANN has been successfully tested.

Because artificial neural networks have been able to estimate the thermal properties of different systems [19] to [21], it was proposed to use them to estimate the thermal conductivity and the heat capacity of an experimental micro-alloyed steel as a function of temperature, and apply them to the thermal analysis of the HAZ. It was decided to design two ANNs, one to estimate the thermal conductivity and the other to estimate the heat capacity. The input neurons in both ANNs were the chemical composition and temperature, and the output neurons were the thermal conductivity and the heat capacity.

1 METHODOLOGY

1.1 Database

The estimation of thermal conductivity is a function of temperature and phases, and these in turn are a function of temperature and chemical composition, which means that a composition of functions exists:

$$k = k(T, \phi), \tag{1}$$

$$\phi = \phi(T, \mu), \tag{2}$$

where k is the thermal conductivity, T is the temperature, ϕ are the phases and μ is the chemical composition. From this, we can see that the thermal conductivity is a function of the temperature and chemical composition:

$$k = k(T, \mu). \tag{3}$$

We can deduce that when the thermal conductivity is determined as a function of the temperature and chemical composition, implicitly the contributions of each phase to the property are considered. The same analysis can be made for the heat capacity.

Table 1. *Minimum and maximum values of chemical composition, the temperature and the thermal conductivity values*

Variable	Minimum	Maximum
%Fe	16.2	100
%C	0.00	1.70
%Mn	0.00	6.00
%Ni	0.00	63.0
%Mo	0.00	4.80
%V	0.00	3.00
%Cr	0.00	30.4
%Cu	0.00	0.64
%Al	0.00	4.50
%Nb	0.00	3.00
%Si	0.00	3.50
%W	0.00	18.5
%Ti	0.00	1.40
%Co	0.00	46.6
Temperature [K]	273	1473
Thermal conductivity [W/(m K)]	10.9	80.2

In research, these properties are used for thermal analysis in unstable state during heating and cooling; however, the relative amount of phases during heating to a given temperature, may differ in the relative amount of phases during cooling at the

same temperature [22], i.e., the thermal properties would be different. It can be concluded that the thermal properties are also a function of the heating and cooling rate, but because there are no studies or data regarding this function, it might be assumed that this function has no influence in the system. Therefore, one search was conducted in the literature to build two databases for metallic materials: one for the thermal conductivity, and the other for the heat capacity, both as a function of the chemical composition and temperature. A careful examination was conducted in order to attain sufficient information to ensure that the chemical composition of the micro-alloyed steel under study was within the limits of the compositions of the collected metallic materials. The collected information for the thermal conductivity and the heat capacity database was conducted by using 395 metallic materials for the former and 176 metallic materials for the latter. Tables 1 and 2 represent the summary for the thermal conductivity and the heat capacity, respectively. In Fig. 1, the behaviour of these two properties for certain selected metallic materials (in this case, steels) are presented. Regarding the thermal conductivity, a greater effect of the chemical composition is observed at low temperatures, being larger for steels with higher contents of alloying elements. Moreover, in relation to the heat capacity, the alloying elements can decrease this property at temperatures between 900 K and 1100 K. This temperature range corresponds to the transformation zone to form austenite; therefore, increasing the heat capacity may be referred to the latent heat of transformation [23].

Table 2. *Minimum and maximum values of chemical composition, the temperature and the heat capacity values*

Variable	Minimum	Maximum
%Fe	21.0	100
%C	0.00	1.70
%Mn	0.00	13.0
%Ni	0.00	60.0
%Mo	0.00	3.60
%Cr	0.00	29.0
%Cu	0.00	0.64
%Al	0.00	4.50
%Nb	0.00	0.90
%Si	0.00	2.00
%W	0.00	18.5
%Ti	0.00	0.60
Temperature [K]	293	1273
Heat capacity [W/(m K)]	402	960

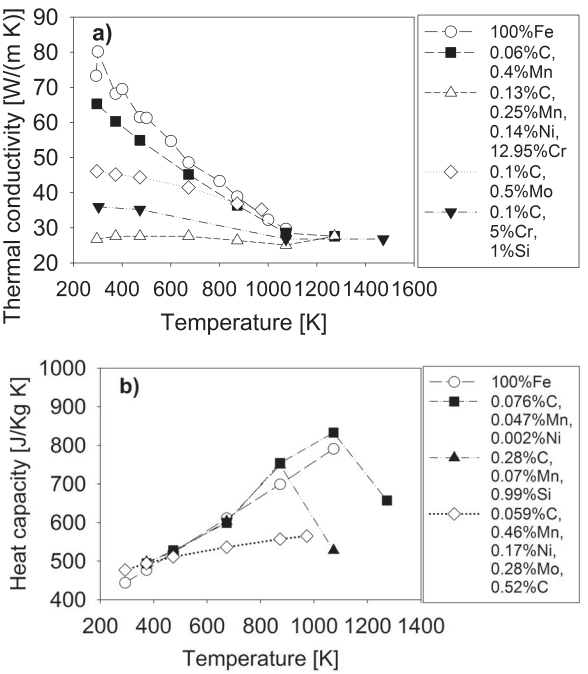

Fig. 1. *Thermal properties as a function of temperature for some steels; a) thermal conductivity, b) heat capacity*

1.2 Design of the ANNs

The ANNs were developed as generalizations of mathematical models of biological neuron systems. The basic unit of an ANN is an elementary processor called a neuron or node, which has the ability to count a weighted sum of its inputs (Eq. (4)), and then apply a transfer function to obtain a signal which is transmitted to another neuron:

$$\left(net\right)_j = \sum_{i=1}^{n} w_{ij} x_i + b, \tag{4}$$

where $(net)_j$ is the weighted sum of the j^{th} neuron for all the n input neurons, w_{ij} is the weight between the neurons of the previous layer and the neurons of the computing layer, b is the bias and x_i is the signal from the i-input neuron.

A transfer function is a function that processes the weighted sum and gives the output signal of the jth neuron. In this work, the sigmoid function was used as a transfer function:

$$f\left(net\right)_j = \frac{1}{1+e^{-(net)_j}}. \tag{5}$$

Through a learning algorithm, the ANNs parameters are adjusted to minimize the mean square error function (E) (Eq. (6)) between the actual outputs and estimate outputs:

$$E = \frac{1}{2}\sum\left(actual\_ouput - estimated\_output\right)^2. \quad (6)$$

Once the error is computed, the weights are updated one-by-one through a back-propagation with a momentum-learning algorithm by Eq. (7):

$$\Delta w_{ij}(i) = -\gamma \frac{\partial E}{\partial w_{ij}} + \alpha \Delta w_{ij}(i-1), \quad (7)$$

where $\Delta w_{ij}(i)$ and $\Delta w_{ij}(i–1)$ are the new and old changes in the weight of the i connection, and γ and α are known as the learning rate and the momentum respectively. In this equation, the function of the momentum is to accelerate the learning rate [14].

In this paper, the design of two ANNs of the multilayer perceptron with a back propagation and momentum learning rule and sigmoid transfer function was proposed. This approach has given good results in predictions based in ANN [9] and [24]. The first ANN was designed to estimate the thermal conductivity, and the second to estimate the heat capacity. In the first, a total of 15 input neurons were used (14 for the chemical composition and 1 for temperature); in the second ANN, a total of 13 input neurons were used (12 for chemical composition and 1 for temperature). All these neurons, both input and output were normalized by using Eq. (8):

$$x_N = \frac{x - x_{\min}}{x_{\max} - x_{\min}}, \quad (8)$$

where x_N is the normalized value of the x neuron, whose maximum and minimum values are $x_{\max}$ and $x_{\min}$ respectively.

Each of the neurons of the input layer corresponds to an input variable (chemical composition and temperature), and each neuron of the output layer corresponds to each output variable (heat capacity or thermal conductivity). Both ANNs were trained with a single hidden layer and different numbers of neurons in this layer. Fig. 2 shows the general architecture of the ANNs.

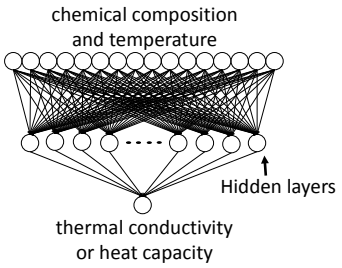

Fig. 2. *Architecture of the ANNs to estimate thermal conductivity and heat capacity*

Each database was divided into two parts. The first one (80 % of the information) was used for the training step, and the second one (20 % of the information) was used for the testing step.

1.3 Materials and Experimental Procedure

We worked with an experimental micro-alloyed steel designated as B2 (yield strength: 788 MPa), which was processed by a thermomechanical process for 11-mm thick producing plates. The chemical composition of the steel is: 0.03%C, 0.24%Si, 1.03%Mn, 0.42%Cr, 0.17%Mo, 1.30%Ni, 0.02%Nb and 0.02%Ti. In order to obtain the carbon equivalent, the Ito-Besseyo for low-C ranges steels was used:

$$P_{cm} = \%\mathrm{C} + \frac{\%\mathrm{Si}}{30} + \frac{\%\mathrm{Mn} + \%\mathrm{Cu} + \%\mathrm{Cr}}{20} + \frac{\%\mathrm{Ni}}{60} + \frac{\%\mathrm{Mo}}{15} + \frac{\%\mathrm{V}}{10} + 5(\%\mathrm{B}). \quad (9)$$

For this steel, the carbon equivalent is 0.15, which indicates that it does not have a tendency to form martensite during the cooling cycle; therefore, preheating was not performed.

In order to determine the effect of thermal cycles produced by welding on microstructure and micro-hardness in this experimental micro-alloyed steel, on a plate of 110 mm × 110 mm × 11 mm, with the gas tungsten arc welding (GTAW) process, an arc was created to simulate a one-pass welding without filler material, which means that a real weld was not made. To ensure the high quality of welding, the welding torch was adapted to a plasma cutting device as shown schematically in Fig. 3. As a result of this adjustment, the welding speed and the distance between the electrode and the plate were settled, keeping them constant. Table 3 shows the parameters used for welding in a single pass. After welding, the plate was left to cool down to room temperature.

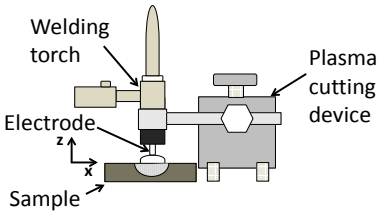

Fig. 3. *Adaptation of the welding torch to plasma cutting device*

To determine the effect of thermal cycles developed during the welding process on the microstructure, a metallographic preparation of welding was performed. This preparation consisted

of obtaining a sample in the transverse direction, in an area away from the boundaries of the beginning and end of the welding zone. To obtain the sample a diamond wheel cutting machine was used (Buehler Isomet 1000), with a controlled low speed to avoid any microstructural changes.

To reveal the microstructure using light microscopy, grinding, polishing, and etching were performed. The sequence of etching was a) 2 % nital during 5 s, b) 2% picral during 3 s and c) 1 % metabisulfite during 20 s. The average grain size in the HAZ was measured by the linear intercept method (ASTM E112). Finally, in accordance with ASTM 384, micro-hardness tests were performed using a Shimadzu Microhardness tester, model HMV-2. The profile of Vickers micro-hardness (HV 0.1) was measured in the welding zone from the FZ to the BM. The measurements were made with a separation of approximately 2.5 footprints.

Table 3. *Welding parameters used*

Current [A]	200
Welding velocity [cm/min]	18
Current type	Direct current electrode negative
Electrode	Tungsten with 2 % Rhodium
Electrode tip shape	pointed
Electrode diameter [mm]	3.18
Distance between plate and electrode [mm]	1.00

1.4 Determination of the Thermal Cycles

It is known that the mechanical properties are functions of the microstructure, and this is a function of the experimental thermal cycles. For this reason, the proposed method by Poorhaydari et al. **[25]** was used to determine the thermal cycles developed during welding, since the experimental determination is a complicated task. The method consists of applying a weight factor to Rosenthal's analytical solutions for thin and thick plates, since most of the welds exhibit an intermediate behaviour between these two categories. This weight factor is determined by:

$$F = \frac{\left(W_{\text{exp}} - W_{Thick-plate}\right)}{\left(W_{Thin-plate} - W_{Thick-plate}\right)}, \qquad (10)$$

where, W_{exp} is the thickness of the experimentally determined HAZ; $W_{\text{Thin-plate}}$ and $W_{\text{Thick-plate}}$ are the thicknesses of the HAZ which are determined from Rosenthal's solutions for thin plate and thick plates, respectively. The weight factor, F, varies from 0 to 1. Values near 0 indicate that the problem is approaching a thick plate, and conversely, when F takes values close to 1, the problem is approaching a thin plate. $W_{\text{Thin-plate}}$ and $W_{\text{Thick-plate}}$ are determined, knowing that in the boundaries between the FZ and the HAZ, and between the HAZ and the BM, the peak temperatures reached during the welding process are known, and which correspond to the melting temperature and the critical temperature A_{c1}, respectively. Poorhaydari showed that the important parameters such as peak temperature and the cooling time between 1073 K and 773 K (commonly known as $t_{8/5}$) can be estimated by weighting the solutions of thick plates and thin plates; that these parameters can be used to correlate microstructure studies and modelling and simulation.

2 RESULTS AND ANALYSIS

After several ANNs with different neurons in the hidden layer were trained, the best fits between the actual and the estimated thermal properties were obtained with 8 neurons. The results of this step for the two ANNs are shown in Fig. 4.

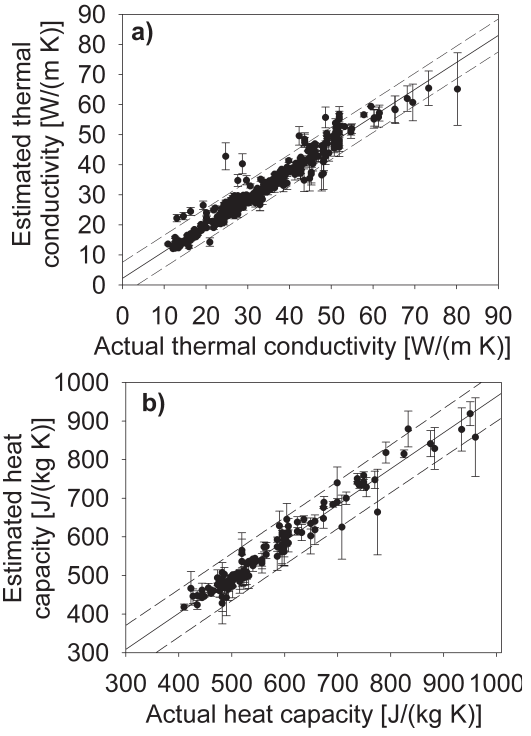

Fig. 4. *Results of the training step; a) thermal conductivity, b) heat capacity*

In this figure, the actual thermal conductivity and the actual heat capacity are compared with those

estimated with the ANNs. In the case of the thermal conductivity, it can be seen that with values higher than 60 W/(m K), an underestimation occurs for this property, but below this value most of the estimated values are close to actual values. For the case of heat capacity, it is observed that at values greater than 800 J/(kg K), there are both underestimation and overestimation of the data.

To determine the efficiency of the ANNs, the linear correlation coefficients were calculated, which are 0.94 for the thermal conductivity and 0.95 for the heat capacity. With these, it is considered that the ANNs have been trained.

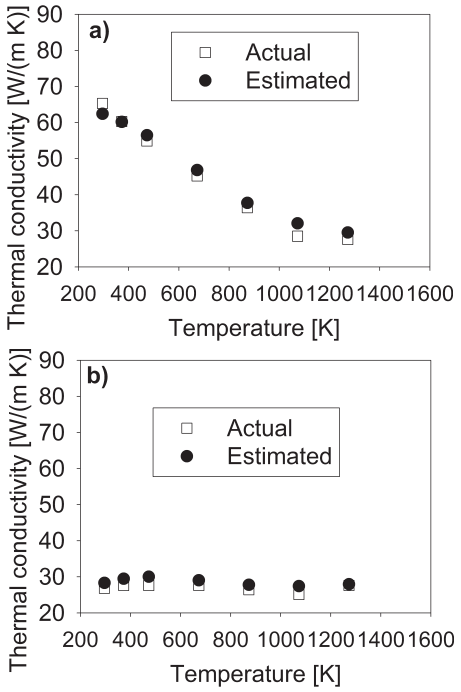

Fig. 5. *Comparison of actual and estimated thermal conductivity by using the ANN, for two different steels; a) 0.06%C, 0.4%Mn; b) 0.13%C, 0.25%Mn, 0.14%Ni, 12.95%Cr*

Once the ANNs have been trained, the thermal properties of the metallic materials that were not used in the training step were estimated in the testing step, but their actual thermal properties are already known. In Fig. 5, the actual and the estimated thermal conductivity by using the ANN are compared for two steels with different thermal behaviour as a function of temperature. In this figure, it can be seen that the ANN was able to estimate the thermal conductivity for both a non-alloy steel (Fig. 5a) and an alloyed steel (Fig. 5b). For the alloyed steel (i.e. ferritic stainless steel), the conductivity is not a strong function of temperature, which could be due to the fact that the ferritic phase is presented in all this temperature range. As in the case of the thermal conductivity, Fig. 6 compares the actual and the estimated heat capacity by using the respective ANN for two different steels that have different thermal behaviour as a function of temperature. As can be seen in Fig. 1b, heat capacity, depending on the steel, may or may not present a maximum around 900 K and 1100 K, which (as already mentioned), it may be due to the latent heat; however, the ANN is able to estimate this behaviour (Fig. 6a). As can be observed from Fig. 6, a good approximation between the actual and the estimated heat capacity is obtained. With these results, it is considered that the ANNs have been tested.

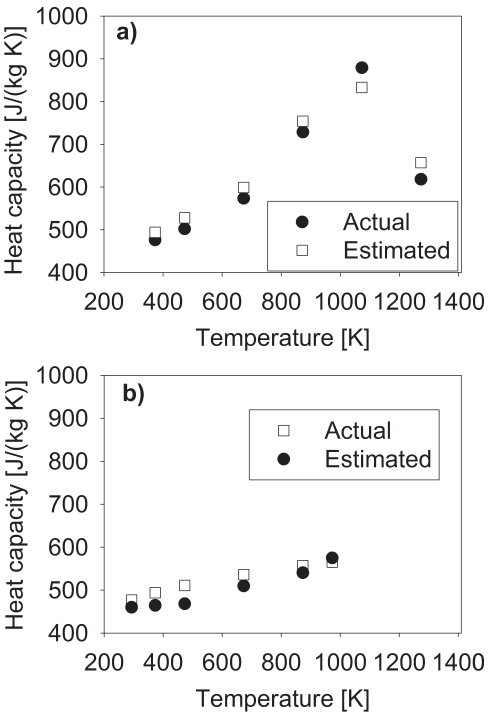

Fig. 6. *Comparison of actual and estimated heat capacity by using the ANN, for two different steels; a) 0.08%C, 0.05%Mn, 0.002Ni, b) 0.059%C, 0.46%Mn, 0.17%Ni, 0.28%Mo, 0.52%Cr*

Once the ANNs were trained and tested, the thermal properties of the micro-alloyed steel under study were estimated. The chemical composition of the micro-alloyed steel and the range of temperatures between 298 K and 1473 K, for the thermal conductivity, and the range of temperatures between 298 K and 1273 K for the heat capacity, were used as input neurons to estimate these thermal properties. Fig. 7 presents the results of the estimated thermal conductivity and the estimated heat capacity. From Fig. 7a, a maximum value of thermal conductivity

about 46 W/(m K) at room temperature is observed, with a tendency to decrease with the temperature until a stable value of approximately of 30 W/(m K) at 1073 K. Regarding the heat capacity (Fig. 7b), a high dependence on this property with temperature can be seen, reaching a maximum of 800 J/(kg K) at 1073 K; after this temperature, a decrease in this property is observed, until a minimum value of 402 J/(kg K) at 1273 K. With these results, it can be seen that this steel has thermal properties similar to that of an alloyed steel.

Fig. 8 presents the microstructures produced by the effect of the welding thermal cycles. The BM, the subzones of the HAZ: inter-critical heat effected zone (ICHAZ), recrystallization heat-affected zone (RCHAZ), coarse grained heat-affected zone (CGHAZ), partially melted heat-affected zone (PMHAZ), and the FZ can be seen. In the BM, microstructural changes are not observed, because the peak temperature reached in this zone was lower than the transformation critical temperature A_{c1}. The microstructure in this zone is composed mainly of acicular ferrite (AF) and quasi-polygonal ferrite (QPF), in addition to the presence of precipitates, which appear as dark particles on etchings with picral. The peak temperatures attained at the ICHAZ were between A_{c1} and A_{c3}; thus, a fraction of the ferrite of the original microstructure was transformed to austenite during heating; during the cooling cycle, the austenite transformed to ferrite. Additionally, in this subzone it can be seen a refining ferrite grain size, untransformed QPF and growth and agglomeration of

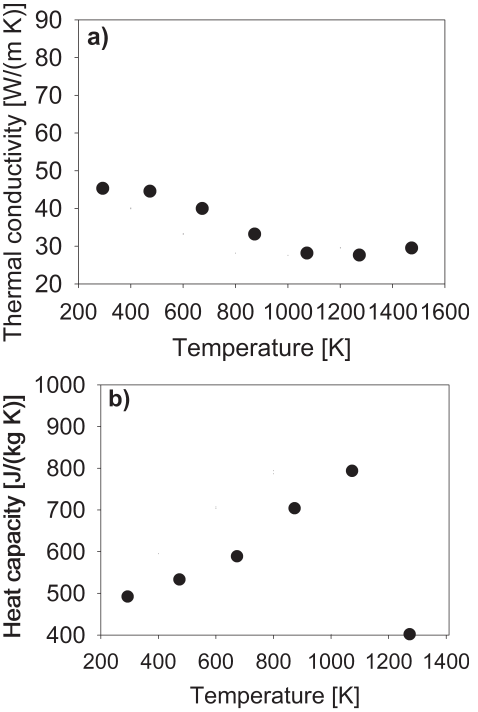

Fig. 7. *Estimated thermal properties for the experimental micro-alloyed steel; a) thermal conductivity, and b) heat capacity, by using the two ANNs*

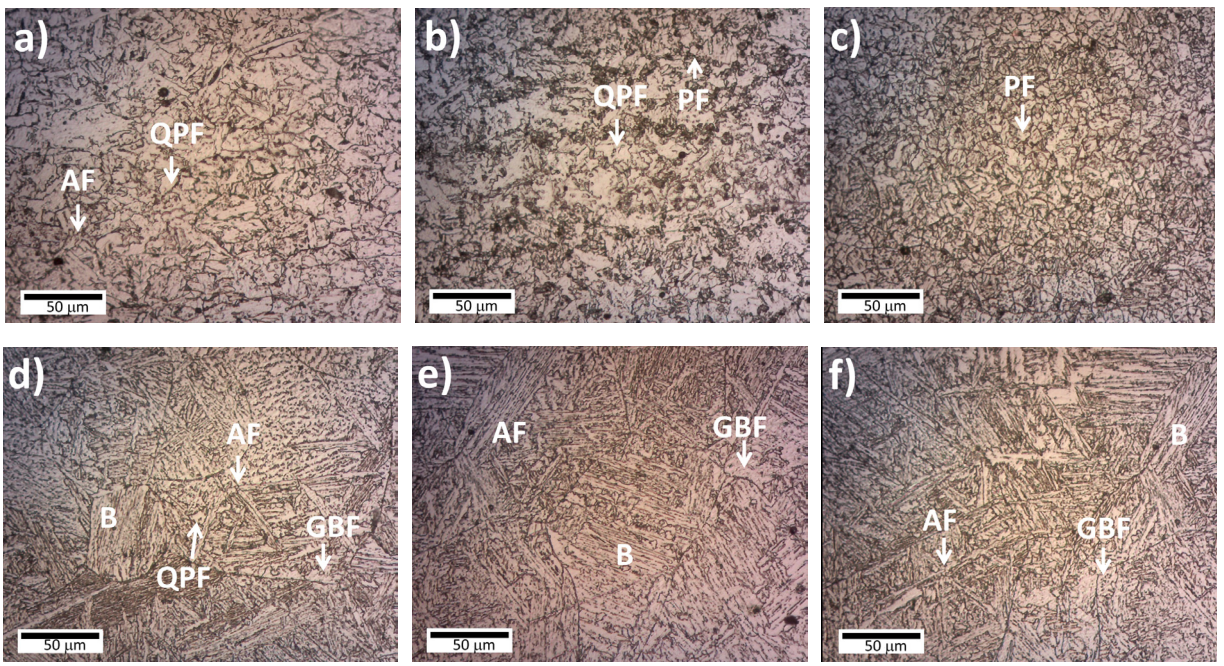

Fig. 8. *Microstructures of the welding zone: a) BM, b) ICHAZ, c) RCHAZ, d) CGHAZ, e) PMHAZ and f) FZ*

precipitates. The RCHAZ reached a peak temperature above A_{c3} but lesser than 1473 K; thus, all the original microstructure transformed to austenite during heating, resulting in the final refined microstructure of polygonal ferrite (PF) grains. In the CGHAZ, a grain coarsening with a microstructure of AF, QPF, grain boundary ferrite (GBF) and bainite (B) can be seen. In the PMHAZ, epitaxial grains and columnar grains that grew in the direction of the heat extraction are observed, in which these grains are composed of a mixture of AF, GBF and B. In the FZ, AF, GBF and B can be seen.

From Fig. 9, it can be seen that the micro-hardness increases in the HAZ from the BM to FZ. In the case of the RCHAZ, this increment is due to the grain refinement, but for the case of the CGHAZ, the increase in micro-hardness is mainly due to the formation of bainite, since in this subzone the grain is over 20 times higher.

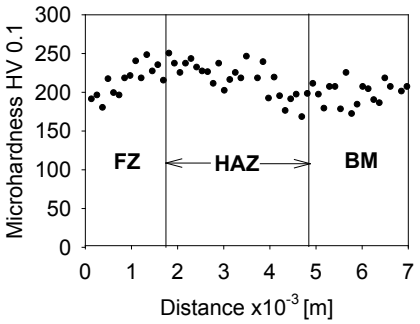

Fig. 9. *Microhardness profile measured in the welding zone*

Once the thermal properties of the experimental micro-alloyed steel were obtained, these were used to determine the peak temperatures and thermal cycles experimented in the HAZ, by solving the Rosenthal's equations and the method proposed by Poorhaydari et al. **[25]**. Fig. 10 shows the peak temperatures determined in the HAZ and BM, and its relationship with the grain size. It is noted that in the CGHAZ, a grain size between 30 μm and 115 μm was obtained; in the RCHAZ a grain size between 5 μm and 20 μm. From this same figure, it can be seen that the grain grew rapidly in the CGHAZ. According to the carbonitride dissolution temperature (Eq. (11) **[26]**), which for this steel is 1273 K, this rapid growth is due to the dissolution of these precipitates **[27]** and **[28]**.

$$\log\left(\left[Nb\right]\left[C+\frac{12N}{14}\right]\right)=2.26-\frac{6770}{T}. \qquad (11)$$

The temperature reached at the BM is less than 993 K, and for this, it did not cause microstructural changes; thus, the micro-hardness was not affected. In the same Fig. 10, the CGHAZ corresponded to peak temperatures between 1473 K and 1807 K; such temperatures cause a coarsening and dissolution of precipitates; grain growth was thus promoted.

From the thermal analysis, the cooling rates experimented in the CGHAZ and RCHAZ were of 69 K/s and 45 K/s, respectively. Thermal analysis showed that the high temperatures reached in the CGHAZ (between 1473 K and 1807 K) induced grain growth, which together with the high cooling rate (69 K/s), favoured the bainite formation. Furthermore, the peak temperatures reached in the RCHAZ (between 996 K and 1473 K), promoted the recrystallization with a grain size between 5 μm and 20 μm; this together with the lower cooling rate (45 K/s) inhibited the formation of bainite.

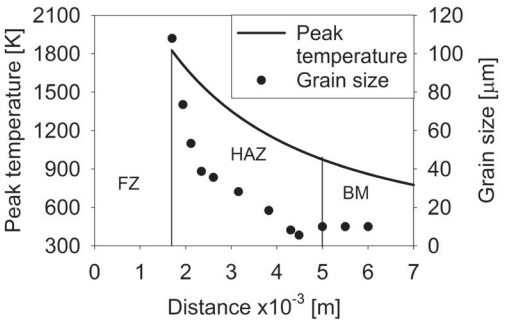

Fig. 10. *Determined peak temperatures and grain size*

3 CONCLUSIONS

Two ANNs were designed, trained and tested to estimate the thermal conductivity and the heat capacity of metallic materials as a function of chemical composition and temperature. The linear correlation coefficients obtained from the comparison between the actual and the estimated values are 0.94 and 0.95 for the thermal conductivity and the heat capacity, respectively.

By testing the ANNs, it was observed that these are able to estimate the thermal properties of any ferrous material that is within the boundaries of the chemical composition and temperature of the database.

Once the ANNs were tested, they were used to predict the thermal properties of an experimental micro-alloyed steel, and these properties were used to estimate the thermal cycles experimented in the HAZ of this same steel. It was observed that the microstructural features and the micro-hardness of the HAZ are functions of the experimented thermal

cycles. The microstructure in the HAZ changes from acicular ferrite, polygonal ferrite, grain boundary ferrite and bainite in the CGHAZ to polygonal ferrite in the RCHAZ. Additionally, in the HAZ and FZ, martensite was inhibited. Due to these microstructures that are functions of the thermal cycle, the CGHAZ showed the hardest zone, although there is no great difference of micro-hardness in the welding zone.

4 ACKNOWLEDGEMENTS

The authors are grateful to CONACyT (grant 178777 and 178511) for the financial support and for the scholarship (No 174555) to E. L.-M. The authors would also like to thank to UNAM PAPIIT grant IN118714 for the final support, and I. Puente-Lee and O. Flores from Faculty of Chemistry-UNAM.

5 REFERENCES

[1] Zinn, W., Scholtes, B. (2002). Residual stress formation processes during welding and joining. Totten, G., Howes, M., Inoue, T. (Eds.) *Handbook of Residual Stress and Deformation of Steel*, ASM International, Ohio, p. 391-397.

[2] Francis, J.A., Bhadeshia, H.K.D.H., Withers P.J. (2007). Welding residual stresses in ferritic power plant steels. *Materials Science and Technology*, vol. 23, no. 9, p. 1009-1020, **DOI:10.1179/174328407X213116**.

[3] Ismar, H., Burzic, Z., Kapor, N., Kokelj, T. (2012). Experimental investigation of high-strength structural steel welds. *Strojniški vestnik - Journal of Mechanical Engineering*, vol. 58, no. 6, p. 422-428, **DOI:10.5545/sv-jme.2011.281**.

[4] de Meester, B. (2001). Development of base materials for welding. *Science and Technology of Welding and Joining*, vol. 6, p. 159-167, **DOI:10.1179/13621710110153870**.

[5] Nazari, A., Milani, A.A., Zakeri, M. (2011). Modeling ductile to brittle transition temperature of functionally graded steels by artificial neural networks. *Computational Materials Science*, vol. 50, p. 2028-2037. **DOI:10.1016/j.commatsci.2011.02.003**.

[6] Lin, Y.C., Liu, G., Chen, M.-S., Zhong, J. (2009). Prediction of static recrystallization in a multi-pass hot deformed low-alloy steel using artificial neural network. *Journal of Materials Processing Technology*, vol. 209, p. 4611-4616, **DOI: 0.1016/j.jmatprotec.2008.10.020**.

[7] Kafkas, F., Karataş, Ç., Sozen, A., Arcaklioğlu E., Saritaş S. (2007). Determination of residual stresses based on heat treatment conditions and densities on a hybrid (FLN2-4405) powder metallurgy steel using artificial neural network. *Materials & Design*, vol. 28, p. 2431-2442, **DOI:10.1016/j.matdes.2006.09.003**.

[8] Hwang, R.-C., Chen, Y.-J., Huang, H.-C. (2010). Artificial intelligent analyzer for mechanical properties of rolled steel bar by using neural networks. *Expert Systems with Applications*, vol. 37, p. 3136-3139, **DOI: 10.1016/j.eswa.2009.09.069**.

[9] Sidhu, G., Bhole, S.D., Chen, D.L., Essadiqi E. (2011). Determination of volume fraction of bainite in low carbon steels using artificial neural networks. *Computational Materials Science*, vol. 50, p. 3377-3384, **DOI:10.1016/j.commatsci.2011.06.032**.

[10] Haque, M.E., Sudhakar, K.V. (2001). Prediction of corrosion–fatigue behavior of DP steel through artificial neural network. *International Journal of Fatigue*, vol. 23, p. 1-4, **DOI:10.1016/S0142-1123(00)00074-8**.

[11] Çöl, M., Ertunç, H.M., Yılmaz, M. (2007). An artificial neural network model for toughness properties in microalloyed steel in consideration of industrial production conditions. *Materials & Design*, vol. 28, p. 488-495, **DOI:10.1016/j.matdes.2005.09.001**.

[12] Castin, N., Fernández, J.R., Pasianot, R.C. (2014). Predicting vacancy migration energies in lattice-free environments using artificial neural networks. *Computational Materials Science*, vol. 84, p. 217-225, **DOI:10.1016/j.commatsci.2013.12.016**.

[13] Echeverri Restrepo, S., Tamayo Giraldo, S., Thijsse, B.J. (2014). Using artificial neural networks to predict grain boundary energies. *Computational Materials Science*, vol. 86, p. 170-173, **DOI:10.1016/j.commatsci.2014.01.039**.

[14] Saric, T., Simunovic, G., Simunovic, K. (2013). Use of Neural Networks in Prediction and Simulation of Steel Surface Roughness. *International Journal of Simulation Modelling*, vol. 12, p. 225-236, **DOI: 10.2507/ijsimm12(4)2.241**.

[15] Seyyedian, Choobi, M., Haghpanahi, M., Sedighi, M. (2012). Prediction of welding-induced angular distortions in thin butt-welded plates using artificial neural networks. *Computational Materials Science*, vol. 62, p. 152-159, **DOI:10.1016/j.commatsci.2012.05.032**.

[16] Ichikawa, K., Bhadeshia, H.K.D.H., MacKay, D.J.C. (1996). Model for solidification cracking in low alloy steel weld metals. *Science and Technology of Welding and Joining*, vol. 1, p. 43-50, **DOI:10.1179/stw.1996.1.1.43**.

[17] Manvatkar, V.D., Arora, A., De, A., DebRoy, T. (2012). Neural network models of peak temperature, torque, traverse force, bending stress and maximum shear stress during friction stir welding. *Science and Technology of Welding and Joining*, vol. 17, p. 460-466, **DOI:10.1179/1362171812y.0000000035**.

[18] Nolan, D., Sterjovski, Z., Dunne, D. (2005). Hardness prediction models based on HAZ simulation for in-service welded pipeline steels. *Science and Technology of Welding and Joining*, vol. 10, p. 681-694, **DOI:10.1179/174329305x65069**.

[19] Erzin, Y., Rao, B.H., Singh, D.N. (2008). Artificial neural network models for predicting soil thermal resistivity. *International Journal of Thermal Sciences*, vol. 47, p. 1347-1358, **DOI:10.1016/j.ijthermalsci.2007.11.001**.

[20] Eslamloueyan, R., Khademi, M.H. (2009). Estimation of thermal conductivity of pure gases by using artificial neural networks. *International Journal of Thermal Sciences*, vol 48, p. 1094-1101, **DOI:10.1016/j.ijthermalsci.2008.08.013**.

[21] Gitifar, V., Abbasi, A., Setoodeh, P., Poursadegh, M., Sahebnazar, Z., Alamdari, A. (2014). Modeling and analysis of the thermal conductivities of air saturated sandstone, quartz and limestone using computational intelligence. *International Journal of Thermal Sciences*, vol. 83, p. 45-55, **DOI:10.1016/j.ijthermalsci.2014.04.015**.

[22] Vuherer, T., Dunđer, M., Milović, L.J., Zrilić, M., Samardžić, I. (2013). Microstructural Investigation of the Heat-Affected

Zone of Simulated Welded Joint of P91 Steel. *Metalurgija*, vol. 52, p. 317-320.

[23] Ortin, J., Planes, A. (1988). Thermodynamic analysis of thermal measurements in thermoelastic martensitic transformations. *Acta Metallurgica*, vol. 36, p. 1873-1889, **DOI:10.1016/0001-6160(88)90291-X**.

[24] Brahme, A., Winning, M., Raabe, D. (2009). Prediction of cold rolling texture of steels using an Artificial Neural Network. *Computational Materials Science*, vol. 46, p. 800-804, **DOI:10.1016/j.commatsci.2009.04.014**.

[25] Poorhaydari, K., Patchett, B.M., Ivey, D.G. (2005). Estimation of Cooling Rate in the Weldign of Plates with Intermediate Thickness. *Welding Journal*, p. 149-155.

[26] Gladman T. (1997). *The Physical Metallurgy of Microalloyed Steels*, The Institute of Materials, London.

[27] Shome, M., Gupta, O.P., Mohanty, O.N. (2004). Effect of simulated thermal cycles on the microstructure of the heat-affected zone in HSLA-80 and HSLA-100 steel plates. *Metallurgical and Materials Transactions A*, vol. 35A, p. 985-996, **DOI:10.1007/s11661-004-0025-8**.

[28] Lei, X.W., Wang, H.H., Wu, K.M., Shirzadi, A.A., Yin, Y.Q., Wu, N.C. (2014). In situ observation of bainite to austenite transformation of microalloyed high strength steel during simulated welding cycle. *Science and Technology of Welding and Joining*, vol. 19, p. 402-407, **DOI:10.1179/1362171814y.0000000205**.